One-dimensional spatial soliton families in optimally engineered quasi-phase-matched lithium niobate waveguides

Roland Schiek, Robert Iwanow, Thomas Pertsch, and George I. Stegeman

Center for Research and Education in Optics and Lasers—School of Optics, University of Central Florida, 4000 Central Florida Boulevard, Orlando, Florida 32816

Gerhard Schreiber and Wolfgang Sohler

Angewandte Physik, Universität Paderborn, 33095 Paderborn, Germany

Received September 24, 2003

The advantage for quadratic soliton generation of engineering the quasi-phase-matching period near the input of lithium niobate slab waveguides is demonstrated. This approach allows members of one-dimensional quadratic soliton families with different values of the wave-vector mismatch to be cleanly excited and to be characterized by quantitative intensity-profile measurements of both the fundamental and the second-harmonic soliton components. © 2004 Optical Society of America

OCIS codes: 190.2620, 190.4390, 190.5530, 190.5940.

Quadratic spatial solitons (QSSs) consisting of a fundamental wave (FW) and its second harmonic (SH) have been investigated both theoretically and experimentally since the mid 1990s.[1,2] Most experiments have used a FW only at the input and relied on propagation into the medium to generate the appropriate SH. In media with a uniform wave-vector mismatch ($\Delta\beta L$), this results in undesirable effects, specifically radiative losses and oscillating components attached to the solitons that decay only slowly with distance. As a result, to date self-trapping has been well studied, but to our knowledge a direct quantitative comparison between measured and calculated intensity profiles of solitons has not been reported.

Quasi-phase matching (QPM) has proved to be a powerful technique for generating QSSs in bulk (two-dimensional) ferroelectric media.[3] It has also been used to study self-trapping in a $LiNbO_3$ slab waveguide (one-dimensional) but the temporal walk-off between the FW and SH and the excitation bandwidth were too large to yield clean spatial solitons.[4] It has been shown theoretically that varying the poling periodicity and hence $\Delta\beta L$ with distance near the input can improve the soliton launching properties.[5] As shown in Fig. 1(a), SH radiative loss and large amplitude oscillations accompany the generation of the QSS's SH component in a waveguide with a uniform $\Delta\beta L$ distribution. Close to phase matching this resulted in launching efficiencies of $<70\%$ in previous experiments.[3,6] In contrast, an optimally engineered QPM grating [see Fig. 1(b) for the variation in the QPM period, Λ, with distance] reduces both the SH radiation and the size and extent of the oscillations forming the steady-state solitons after a few millimeters of propagation. The nonuniform region of the QPM grating serves as an adiabatic SH generator for the QSS's SH. Here we demonstrate QPM engineering to optimize QSS excitation via FW-only launching, which together with detailed modeling leads to measurements of one-dimensional QSS families for comparison with theory.

The measurements were performed on 5-cm-long titanium-indiffused film waveguides on z-cut $LiNbO_3$ samples with propagation along the crystal's x axis. Phase matching between the FW and SH TM_0 modes for a FW wavelength of $\lambda_{PM} = 1552.6$ nm was achieved with electrically poled QPM gratings with a constant periodicity of $\Lambda = 17.6344$ μm at room temperature in the last 4 cm of the sample. In the first 1 cm of the sample the QPM periodicity increased from 17.4800 to 17.6344 μm to form the SH generator. The sample, which was heated in an oven to prevent photorefractive effects, had a temperature gradient toward the colder oven ends, introducing additional nonuniformity in $\Delta\beta L$. Our calculations have shown that adiabatic QSS formation still occurs and a high-quality QSS with its unique steady-state properties propagates in the 3-cm-long central region of the sample. However, the small temperature drop in the last centimeter of the sample introduces a sufficient $\Delta\beta L$ gradient to partially backconvert the SH soliton component into the FW (see Fig. 1). As verified by numerical simulations, neither the FW nor the SH soliton profile changes significantly during the backconversion. Correcting for this energy exchange, we can still measure both profiles at the sample's output facet. A NaCl color-center laser operating at

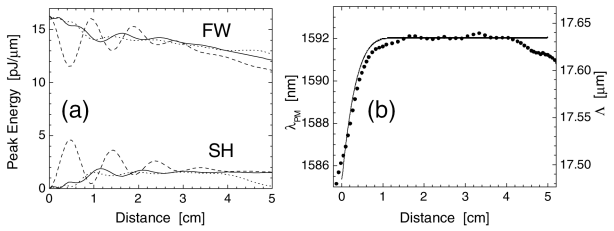

Fig. 1. (a) Evolution of the peak FW and SH energy densities of a pulsed 87-μm-wide QSS at $\Delta\beta L = 7.7\pi$ (dashed curves, uniform QPM; solid curves, optically engineered QPM; dotted curves, measured phase-matching profile). (b) Designed QPM period (solid curve) and measured variation in wave-vector mismatch (dotted curve).

0146-9592/04/060596-03$15.00/0

$\lambda = 1587.5$ nm provided 8.5-ps pulses at a 76-MHz repetition rate. Our laser's narrow spectral width of 0.4 nm is comparable with the acceptance bandwidth of SH generation in a 5-cm-long $LiNbO_3$ waveguide. Laser beams with 0–160-W peak power were launched into the waveguide after shaping with a cylindrical telescope. The waveguide output was imaged into a camera. The time-averaged intensity profiles were measured after scaling of the camera's sensitivity and spatial resolution. Additionally, the powers of the input and the FW and SH output were measured.

Because of the oven, we had access only to data at the waveguide output. For a correct interpretation of the QSS's spatial and temporal evolution inside the crystal it was essential to have a quantitatively correct simulation of our experiment. We used a beam propagation method to solve the time-resolved propagation equations (see, for example, Ref. 1), taking all important experimental details into account. All simulation parameters were measured or calculated from experimental data and checked experimentally. The $\Delta\beta L$ profile was measured with a noncollinear SH-generation technique.[7] The excellent agreement between all measured and calculated results verifies the modeling for extrapolating from the measured output data to the spatial and temporal beam characteristics inside the crystal.

We excited solitons by use of different wide FW input beams with Gaussian shapes that resemble closely the shape of the steady-state solitons. We increased the input power until the FWHM of the FW output beam equaled the input beam width. Oscillations that were due to a mismatch of the power–width ratio of the input beam and the evolving soliton's FW component were minimized at this point. Figure 2 shows the smooth monotonic narrowing of the FW output beam versus input peak power, which contrasts with the oscillating beam width versus intensity observed previously in uniform QPM gratings.[3] The observed output profiles in Fig. 3 are typical for soliton experiments with pulsed excitation and time-averaged imaging. Light at and near the pulse's peak is trapped in a soliton, but the weak pulse wings diffract. The diffracting light appears in the time-averaged FW output profile as a small shoulder underlying the soliton.

It was recently shown that the temporally averaged SH output spatial profiles need to be interpreted carefully because of walk-off effects caused by unequal FW and SH group velocities.[4] As phase matching is approached, the SH component of the soliton increases and an increasing part of the measured SH profile no longer belongs to the soliton but represents SH radiation that has temporally walked away from it. Figure 4 shows the calculated output time–space distribution of the soliton intensity. The spatial narrowing of the FW forming the soliton in the pulse center is evident. Based on simulations we estimated the amount of walked-off SH. Most of the SH temporally overlaps the FW pulse and belongs to the soliton. Weak SH radiation trails the soliton by up to the 17-ps walk-off time. For $\Delta\beta L < 6\pi$ the walked-off SH dominates the SH output, and reliable measurements of the QSS's SH profile are not normally possible with time-averaged intensity outputs with our 8.5-ps pulses. The simulations also show that the QPM engineering suppresses part of the walked-off SH that would be larger in a uniform QPM grating.

Experimentally, we were able to distinguish the SH belonging to the soliton from the walked-off SH by measuring the output spectra. Figure 5 compares the spectra of the QSS's SH and FW components. Closer to phase matching an increasing amount of SH radiation is generated, with a peak wavelength equal to half the phase-matching wavelength, λ_{PM}. The soliton's SH spectrum peaks at half the FW peak's wavelength. The ratio between the integrated energies of these two SH peaks can serve as an estimate of the ratio between the radiating and the soliton SHs. For

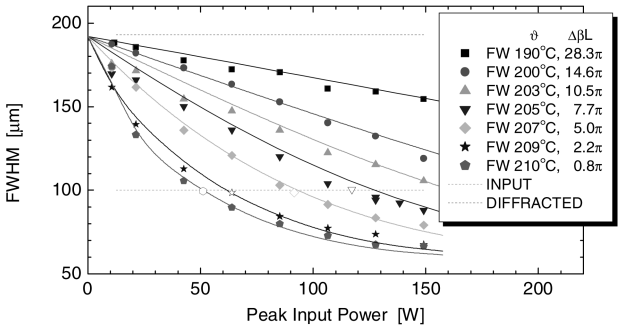

Fig. 2. Output beam narrowing of a 100-μm-wide input beam for increasing input peak power. The solid curves are calculated. The solitons are marked with open symbols. The input and the low power output beam widths are shown with dashed curves.

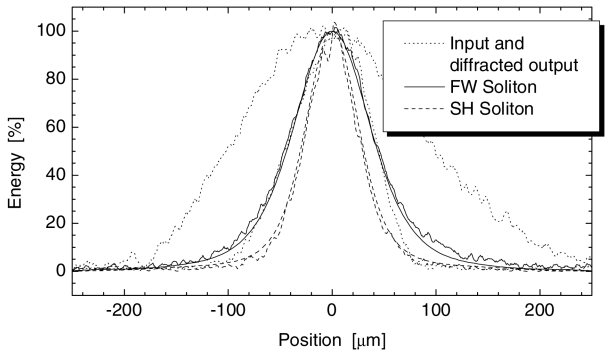

Fig. 3. Normalized energy-density profiles of an 87-μm-wide soliton, phase-mismatch $\Delta\beta L = 7.7\pi$ at 205 °C. Noisy curves are experimental and smooth curves are simulated.

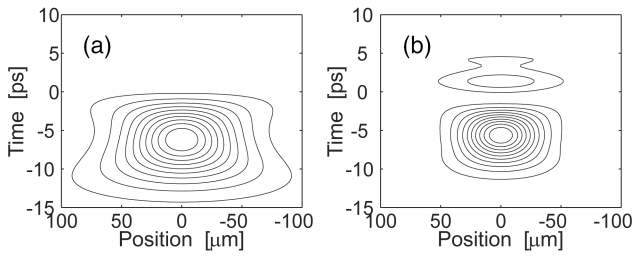

Fig. 4. Calculated time–space intensity distribution of the output beam, 87-μm-wide soliton at $\Delta\beta L = 7.7\pi$. (a) FW, (b) SH.

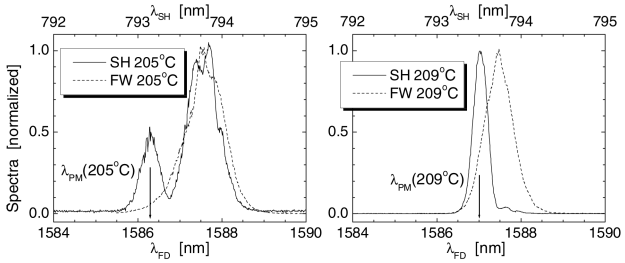

Fig. 5. Normalized FW and SH spectra of 87-μm-wide solitons at 205 °C and 209 °C ($\Delta\beta L = 7.7\pi$ and $\Delta\beta L = 2.2\pi$, respectively).

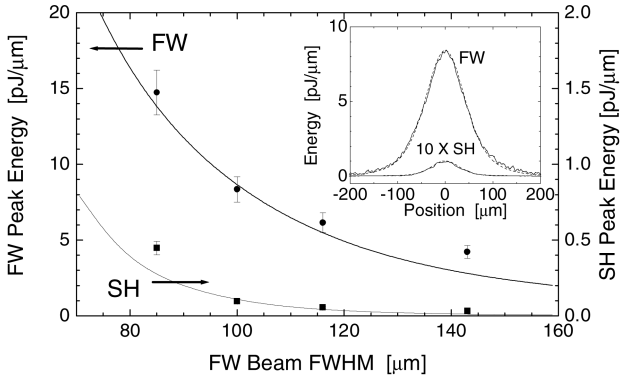

Fig. 6. Soliton family for $\Delta\beta L = 7.7\pi$: pulse energy per micrometer in the beam center versus the FWHM of the soliton. The solid curves are theoretical. The inset shows the output profiles of the 100-μm-wide soliton.

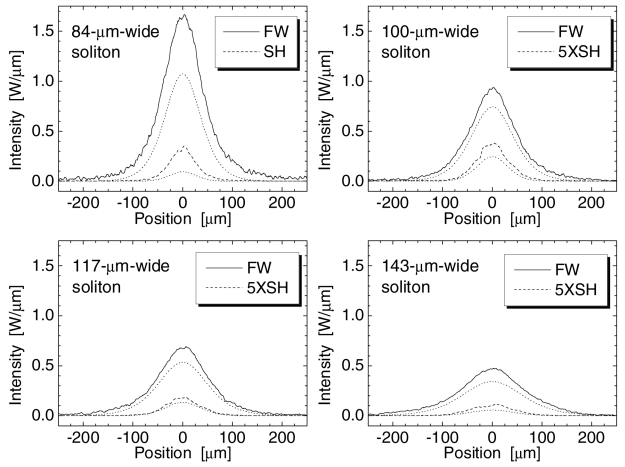

Fig. 7. Pulse peak intensities of the FW and SH parts of measured soliton family members compared with cw eigenmode solutions (dotted curves), $\Delta\beta L = 7.7\pi$ at 205 °C. Where indicated, the SH is magnified $\times 5$ for clarity.

$\Delta\beta L > 7.7\pi$ below 205 °C, more than 75% of the output SH belongs to the soliton, in agreement with the time–space simulation results shown in Fig. 4.

QSSs form a one-parameter soliton family, i.e., they are specified completely by one of two parameters: peak intensity and spatial width for a given phase mismatch. In Fig. 6 the measured pulse energy per micrometer of beam width in the beam center versus the FWHM of the soliton's FW for the family with $\Delta\beta L = 7.7\pi$ is compared with calculations. In the inset the pulse-energy profiles of a 100-μm-wide soliton measured at the output facet are shown to be in excellent agreement with theory. As indicated in Fig. 3, there is negligible background spatially underlying the soliton, so the measured output, reduced by the walked-off SH, belongs completely to the soliton. Comparing the measured powers of the input and output beams, we find that the soliton and the walked-off SH at the output contained in total 88% of the launched power. Taking the 90% throughput and the <5% walked-off SH into account, this corresponds to a soliton launching efficiency of >93%.

To compare the measured beams with the intensity profiles of ideal cw solitons, we transform the energy profiles approximately to peak intensity profiles by division by 9 ps for the FW and by 6.4 ps for the SH effective pulse lengths, neglecting walk-off and assuming Gaussian pulses. Figure 7 compares the four measured solitons of the family at $\Delta\beta L = 7.7\pi$. The narrower pulsed solitons have an increasingly larger peak intensity than the cw solitons because the pulse wings are more strongly diffracting. The measured SH part of the soliton is corrected by a factor of 5 to compensate for the (calculated) SH backconversion near the sample output (see Fig. 1). The agreement between the measured and calculated soliton profiles is reasonable and is the best that can be expected in pulsed soliton experiments.

The launching of quadratic solitons into $LiNbO_3$ slab waveguides that are wave-vector matched via QPM engineering for optimum soliton excitation has been demonstrated. The resulting improvements in the launching process, together with detailed spatiotemporal modeling, allowed the detailed properties of the soliton families to be measured. Excellent agreement with theory was found.

The research was supported by the European Commission (Information Society Technologies Programme/Future & Emerging Technologies), the National Science Foundation, and a U.S. Army Research Office Multidisciplinary University Research Initiative.

References

1. C. Etrich, F. Lederer, B. A. Malomed, T. Peschel, and U. Peschel, in *Progress in Optics*, E. Wolf, ed. (Elsevier, New York, 2000), Vol. XLI, pp. 483–568.
2. A. V. Buryak, P. Di Trapani, D. Skryabin, and S. Trillo, Phys. Rep. **370,** 63 (2002).
3. H. Kim, L. Jankovic, G. I. Stegeman, S. Carrasco, L. Torner, D. Eger, and M. Katz, Opt. Lett. **28,** 640 (2003).
4. P. Pioger, V. Couderc, L. Lefort, A. Barthelemy, F. Baronio, C. De Angelis, Y. Min, V. Quiring, and W. Sohler, Opt. Lett. **27,** 2182 (2002).
5. S. Carrasco, J. P. Torres, L. Torner, and R. Schiek, Opt. Lett. **25,** 1273 (2000).
6. E. Lopez-Lago, C. Simos, V. Couderc, A. Barthelemy, D. Artigas, and L. Torner, Opt. Lett. **26,** 1277 (2001).
7. T. Pliska, F. Mayer, D. Fluck, P. Günter, and D. Rytz, J. Opt. Soc. Am. B **12,** 1878 (1995).